Journal of Materials Chemistry B

Accepted Manuscript

ROYAL SOCIETY OF CHEMISTRY

www.rsc.org/materialsB

Journal Name

RSCPublishing

ARTICLE

Conjugation of multivalent ligands to gold nanoshells and designing a dual modality imaging probe

Cite this: DOI: 10.1039/x0xx00000x

Mathieu Bedard,[a,§] Pramod K. Avti,[a,b,c,d,§] Tina Lam,[a] Leonie Rouleau,[e] Jean-Claude Tardif,[c,f] Eric Rhéaume,[c,f,*] Frederic Lesage[b,c,*] and Ashok Kakkar[a,*]

Received 00th January 2012,
Accepted 00th January 2012

DOI: 10.1039/x0xx00000x

www.rsc.org/

Design and synthesis of branched tetraethylene glycol (TEG) based ligands for subsequent conjugation to gold nanoshells, are reported. TEG enhances aqueous solubility of hollow gold nanoshells (HAuNSh), and the branched architecture provides stability. An examination of the supernatant of the surface displacement reaction shows that the structure of the ligand plays an important role during functionalization of HAuNSh. The binding of multivalent ligands leads to rupturing of the gold nanoshell architecture due most probably to the large dendron not compensating the replacement of small citrate capping agents. The construction of a probe with dual imaging capabilities is demonstrated by covalent linking of a dendron containing $Cy5.5_A$ dye to gold nanoshells. It leads to fluorescence quenching of $Cy5.5_A$ by the gold nanoshells, as evidenced in solution and in cellular internalization studies with J774 and bEnd.3 cells.

1. Introduction

Among the repertoire of metal nanoparticles, gold nanoshells (AuNSh) have offered tremendous potential in designing novel materials for biomedical applications.[1] Core-shell based AuNSh, especially those built on silica nanoparticles, have been extensively explored as immunoassays, and for thermoablation, cancer therapy, cell labelling etc.[2] Gold nanoshells without any core (hollow, HAuNSh) have also become a topical area of research due to their increased absorption cross section.[3] HAuNSh provide an attractive venue in developing near-infrared contrast agents for biological imaging. During their synthesis, HAuNSh are stabilised using citrate as a capping agent.[4] The scope of these nanomaterials can be further enhanced by their surface functionalization, leading to increased solubility, stability, targeting, and for delivering active therapeutic agents.[5] This is generally achieved by a displacement reaction using an appropriate thiol terminated ligand, which binds strongly to gold on the nanoshell surface.[6] Multivalent ligands such as dendrons provide opportunities to enhance the efficacy of surface coverage by introducing greater number of desired moieties in fewer displacement reactions.[7] We report the design of such branched architectures containing tetraethylene glycol (TEG) in the backbone and the surface, which are subsequently conjugated to gold nanoshells through the thiol moiety at their core. Oligoethylene glycols such as TEG provide hydrophilic environment which enhances aqueous solubility and dispersion of nanoparticles. We demonstrate that the shape of the ligand (linear vs branched) plays a significant role in the routinely used surface coating process, and a careful examination of the supernatant in ligand displacement reactions on metal nanoparticles is essential to determine the efficiency of this reaction.

Combination of surface plasmon resonance of gold nanoshells with the fluorescence of dyes operating in the therapeutic window, constitutes an important platform in developing dual imaging probes for improved diagnostics.[8] We designed a dendron based ligand containing an analog of Cy5.5 dye ($Cy5.5_A$) which upon conjugation to the gold nanoshell surface leads to their easy dispersion in an aqueous medium, and quenching of the fluorescence of $Cy5.5_A$. Our dendron based methodology provides a simple, efficient and a versatile route to introduce desired functionalities on to gold nanomaterials, and in developing integrated dual imaging modalities.

2. Experimental

2.1 Materials and Methods: The compounds trisodium citrate, sodium borohydride, gold(III) chloride hydrate, tetraethylene glycol, p-toluenesulfonyl chloride, sodium hydroxide, sodium hydride, thioacetic acid, 4-dimethylaminopyridine, methylsulfonyl chloride, triethylamine, sodium azide, tetrabutylammonium iodide, lithium hydroxide, pentynoic acid, sodium ascorbate, copper(II) sulfate hexahydrate, borane-THF,

bis(triphenylphosphine)palladium(II) dichloride, propargyl bromide, (triisopropylsilyl) acetylene, (trimethylsilyl) acetylene, potassium thioacetate, methyl 3,4,5-trihydroxybenzoate, sodium thiomethoxide (Sigma Aldrich), 1-Ethyl-3-(3-dimethylaminopropyl)carbodiimide ≥98% (Fluka), cobalt(II) chloride hexahydrate (Fisher Scientific), hydrochloric and nitric acid (ACP Chemicals), PEG_{750} (Alfa Aesar), and 3-bromo-5-iodobenzoic acid 98% (AK Scientific Inc.), were used as received. 400 square-Mesh copper grid was purchased from Electron Microscopy Science. Ultrapure water was doubly distilled by reverse osmosis though a Millipore RiOS 8, followed by filtration through a MilliQ Academic A10 unit. Acetonitrile was dried over calcium hydride.

NMR acquisition was carried out on a 300 or 400 MHz Varian Mercury instrument and operated using VNMRJ 2.2D software. Mass spectral analyses (MS and MALDI-TOF) were performed on a Kratos MS25RFA high resolution mass spectrometer. UV-Vis and fluorescence spectra were obtained on Cary 500 UV-Vis and Cary Eclipse Fluorimeter, respectively. TEM analyses were carried out on Tecnai 12 TEM with AMT XR80C CCD Camera, and the TEM images were in bright-field mode at an accelerating voltage of 120 kV. Samples were prepared by placing a small droplet of AuNSh solution on a CF400-Cu Carbon Film of a 400 square-Mesh copper grid, and the image acquired from TEM were processed using ImageJ software. Thermogravimetric analysis was performed on a TGA Q500 V6.7 Build 203 instrument. Samples for TGA were prepared by freezing the conjugated gold nanoshell solution at -78°C, followed by lyophilization overnight. The solid (approximately 0.25-0.35 mg) was then collected, weighed onto a platinum pan, and subjected to TGA under a flow of air. The temperature was ramped at a rate of 20°C/min to 100°C and held at isotherm for 2 min. It was then increased to 500°C at the same rate, at which point a flow of nitrogen replaced air and the temperature raised to 700°C. Air and N_2 flow rates were set at 40 $mL \cdot min^{-1}$ and 60 $mL \cdot min^{-1}$, respectively. The primary weight loss is attributed to the thiolated ligand. Calculations were performed[3a] using the percentage of weight lost due to the organic ligand obtained from TGA to approximate the amount of ligand originally present on the surface of the AuNSh.

2.1 Gold nanoshell synthesis

Hollow gold nanoshells were prepared by adapting a procedure reported earlier,[3a,4a] and is briefly described here. The glassware used in the synthesis was soaked in a 3:1 mixture of $HCl:HNO_3$ (aqua regia) for 1h, rinsed with ultrapure water 3 times, and dried in an oven overnight. In a 2L 3-necked round bottom flask, 1.5 L of MilliQ H_2O were degassed and filled with Ar by repeating the cycle of evacuation and filling with Ar 4 times. To this flask kept under a positive flow of Ar, trisodium citrate (1.2345 g, 4.20 mmol) was added, and the cycle of evacuating and filling with Ar was repeated once more. While keeping a positive flow of Ar, cobalt(II) chloride hexahydrate (150 mg, 0.630 mmol) was added and the mixture was stirred vigorously. Sodium borohydride ($NaBH_4$, 142.5 mg, 3.77 mmol) was dissolved in approximately 2 mL of degassed MilliQ water, and added *via* syringe injection to the above cobalt solution while stirring vigorously. The reduction of the cobalt salt leading to the formation of cobalt nanoparticles was indicated by a rapid color change from faint purple to near-black. The formation of H_2 gas bubbles was the visual cue for monitoring the completion of the reaction. In another 3L 3-neck round bottom flask, 900 mL of MilliQ H_2O was degassed and filled with Ar in four cycles. Gold(III) chloride hydrate ($HAuCl_4$ – 12mg, 0.0353 mmol) was dissolved in 2 mL of degassed MilliQ water, and added to this 3 L flask *via* syringe injection. The cobalt solution was rapidly transferred to the 3-neck flask under a positive Ar flow. The mixture was left to react for 10 mins and then opened to air for 4 hours. Its green/grey color indicated the formation of gold nanoshells. The solution was concentrated by centrifugation at 4600 rpm at 4°C for 2 hours in separate tubes. The supernatants were recombined, followed by a second cycle of centrifugation for 3 hours at 4600 rpm at 4°C.

2.2 Monofunctional ligand containing a protected thiol entity, tetraethylene glycol thioacetate (G0-TEG-SAc), was prepared using an adaptation of the literature procedure.[9]

Synthesis of Multivalent Ligands

2.2.1 TEG-Ts (1) was prepared by adapting a procedure reported by Ashton *et al.*.[9d] TEG (17.56 g, 90.4 mmol) was dissolved in THF (2.5 mL) in a 500 mL three-necked round bottom flask under Ar atmosphere. NaOH (1.085 g, 27.12 mmol) was dissolved in a minimal amount of water and added to the TEG solution. The resulting mixture was stirred for 2 minutes and then cooled to 0°C. Subsequently, freshly purified TsCl (3.45 g, 18.08 mmol) was dissolved in THF (10 mL) and added dropwise (*via* an addition funnel under Ar atmosphere) to the TEG solution while stirring vigorously. Once the addition was complete, the reaction mixture was stirred for 2h. THF was removed under reduced pressure and an ice-water slurry (20 mL) was added. The product was extracted with DCM (60 mL) and the organic phase was washed with brine (10 mL) and dried over $MgSO_4$. The crude product was concentrated *in vacuo*, and was purified using column chromatography with EtOAc to give a colorless, transparent oil (4.08 g, 65%). ^1H NMR (300MHz, $CDCl_3$): δ 2.44 (s, 3H), 3.75-3.51 (m, 14H), 4.21-4.11 (m, 2H), 7.34 (d, 2H), 7.79 (d, 2H) ppm.

2.2.2 TEG-SAc (2) was prepared by adapting a procedure reported earlier.[10] TEG-Ts (0.70 g, 2.00 mmol) was dissolved in dry DMF (3 mL) in a 50 mL Schlenk under Ar atmosphere. Potassium thioacetate (0.69 g, 6.03 mmol) was added after cooling at 4°C and the mixture was stirred vigorously for 20 hours. HCl (5% v/v, 20mL) was added dropwise while stirring. The product was extracted with EtOAc (4 x 40 mL) and the combined organic phases were washed with H_2O (3 x 10 mL), brine (1 x 10 mL) and then dried over $MgSO_4$. The crude product was concentrated *in vacuo* and purified using flash chromatography with Et_2O/MeOH (100:0, 95:5, 90:10, 85:15, 80:20) as eluent, with the majority of the product eluting with 85:15. The product was concentrated under reduced pressure to

give an orange viscous oil (0.260 g, 51%) which was stored under Ar atmosphere at 4°C. ^{1}H NMR (400MHz, $CDCl_3$): δ 2.34 (s, 3H), 3.10 (t, 2H), 3.58-3.67 (m, 12H), 3.73 (t, 2H) ppm.

2.2.3 Methyl 3,4,5-tris(prop-2-ynyloxy)benzoate (3): A mixture of methyl 3,4,5-trihydroxybenzoate (6.42g, 34.86 mmol), K_2CO_3 (19.28g, 174.3 mmol) and propargyl bromide (20.73g, 174.3 mmol) in DMF (50 mL) was stirred vigorously for 5 days. Excess propargyl bromide was removed *in vacuo*. H_2O (125 mL) was added and the product extracted with EtOAc (4 x 75 mL). The collected organic phases were washed with H_2O (3 x 75 mL) and brine (3 x 75 mL), dried over K_2CO_3, and the solvent was removed to give a brittle off-white solid (9.56g, 92%). ^{1}H NMR (300MHz, $CDCl_3$): δ 2.46 (t, 1H), 2.53 (t, 2H), 3.91 (s, 3H), 4.81 (2d, 6H), 7.47 (s, 2H) ppm. ^{13}C NMR (300MHz, $CDCl_3$): δ 52.37, 57.03, 60.31, 76.59, 78.66, 109.78, 125.74, 141.01, 151.26, 166.24 ppm.

2.2.4 3,4,5-Tris(prop-2-ynyloxy)benzoic acid (Dendron-Acid-Trip, **4**)**:** A solution of **3** (1g, 3.35 mmol) in THF was vigorously stirred with 4M $KOH_{(aq)}$ (20 mL) for 2 days. The solution was acidified to pH = 3 with HCl (37% v/v), and the product was extracted with THF (3 x 10 mL). The collected organic phases were washed with brine (2 x 8 mL), dried over $MgSO_4$ and the solvent was removed *in vacuo* to give a brittle off-white solid (0.81 g, 85%). ^{1}H NMR (300MHz, DMSO): δ 3.48 (t, 1H), 3.62 (t, 2H), 4.71 (d, 2H), 4.89 (d, 4H), 7.38 (s, 2H), 13.06 (s, 1H) ppm. ^{13}C NMR (300MHz, $CDCl_3$): δ 56.90, 59.92, 78.80, 79.53, 109.29, 126.70, 140.10, 151.37, 167.09 ppm.

2.2.5 Dendron-TEG-SAc-Trip (5): Compound **4** (0.234 g, 0.826 mmol) and TEGSAc (0.250 g, 0.991 mmol) were dissolved in dry DCM (8 mL) in a 50 mL Schlenk flask under an Ar atmosphere. DMAP (0.151 g, 1.24 mmol) was added and the mixture was stirred for 5 minutes. EDC (0.141 g, 0.908 mmol) was added and the mixture was stirred for 2 days. The solvent was removed *in vacuo*, and the crude product was purified using flash chromatography with DCM/MeOH (99:1). The solvent was removed *in vacuo* to give an orange-brown oil (0.31 g, 72%). ^{1}H NMR (300MHz, $CDCl_3$): δ 2.32 (s, 3H), 2.52 (t, 1H), 2.55 (t, 2H), 3.09 (t, 2H), 3.57-3.70 (m, 12H), 3.83 (t, 2H), 4.47 (t, 2H), 4.80 (d, 4H), 4.82 (d, 2H), 7.49 (s, 2H) ppm. ^{13}C NMR (300MHz, CDCl3): δ 28.71, 30.55, 57.16, 60.32, 64.52, 69.22, 69.74, 70.30, 70.58, 70.12, 70.77, 75.58, 76.26, 110.14, 125.74, 141.23, 151.30, 165.69, 195.50 ppm. Expected mass: 518.58 g·mol^{-1}, ESI m/z = 519.17 g·mol^{-1}.

2.2.6 G1-3-TEGOH (6): Dendron-TEG-SAc-Trip (**5**, 0.106 g, 0.204 mmol), N_3TEG[3a] (0.134 g, 0.613 mmol) and sodium ascorbate (0.012 g, 0.061 mmol) were dissolved in THF (1 mL) in a 50 mL Schlenk flask under Ar. $CuSO_4$ was added and the mixture was stirred vigorously for 2 days at 40°C. The solvent was removed *in vacuo*. The product was extracted in DCM (5 mL) and stirred with EDTA (100 mg) for 2 hours. This process was repeated twice. The mixture was dried over Na_2SO_4 and filtered. The solvent was almost entirely removed *in vacuo* (leaving only approximately 2 mL). Et_2O was added dropwise to precipitate the oily product. When the orange solution ceased being cloudy, the mixture was decanted. The orange oil was dissolved in DCM (2 mL) and the precipitation was repeated. The remaining DCM was removed *in vacuo* to yield an orange oil (0.095 g, 39%). ^{1}H NMR (400MHz, $CDCl_3$): δ 2.32 (s, 3H), 3.07 (t, 2H), 3.32 (s, broad, 7H), 3.56-3.62 (m, 46H), 3.68-3.72 (m, 14H), 3.84 (s, 3H), 3.92 (s, 8H), 4.46 (s, 3H), 4.60 (s, 8H), 5.25 (s, 6H), 7.46 (s, 2H), 8.06 (s, 3H) ppm. ^{13}C NMR (300MHz, CDCl3): δ 28.76, 30.52, 50.31, 61.47, 63.13, 64.32, 69.11-69.66, 70.17-70.62, 72.45, 109.39, 124.92-125.02, 125.54, 141.76, 151.97, 165.82, 195.49 ppm. Expected mass: 1176.29 g·mol^{-1}, ESI m/z = 1198.52 g·mol^{-1} [M+Na$^+$].

2.2.7 G2-9-Trip (7) G1-3-TEGOH (**6**, 0.459 g, 1.615 mmol) and **4** (0.380 g, 0.323 mmol) were dissolved in dry CH_3CN (8 mL) in a 50 mL Schlenk flask under Ar atmosphere. DMAP (0.178 g, 1.454 mmol) was added and the mixture was stirred for 5 minutes. EDC (0.166 g, 1.070 mmol) was added and the mixture was stirred for 2 days. The crude product was extracted in DCM (30 mL) and dried over $NaSO_4$. The solvent was removed *in vacuo*. The crude product was purified using flash chromatography with DCM/MeOH (95:5). The solvent was removed *in vacuo* to give a clear yellow oil (0.019 g, 3%). ^{1}H NMR (300MHz, $CDCl_3$): δ 2.32 (s, 3H), 2.47 (s, 3H), 2.57 (s, 6H), 3.07 (t, 2H), 3.58-3.70 (m, 45H), 3.78-3.88 (m, 16H), 4.42-4.54 (m, 9H), 4.52-4.54 (m, 7H), 4.78-4.83 (m, 24H), 5.22 (s, 6H), 7.46 (s, 10H), 7.96 (s, 3H) ppm. ^{13}C NMR (300MHz, CDCl3): δ 28.80, 29.68, 50.25, 53.42, 57.17, 60.31, 64.42, 69.14-69.72, 70.27-70.70, 78.00, 78.67, 110.11, 125.69, 141.21, 151.28, 165.64 ppm. Expected mass: 1975.04 g·mol^{-1}, ESI m/z = 1996.69 g·mol^{-1}[M+Na$^+$].

2.2.8 G2-9-TEGOH (8): G1-9-Trip (**7**, 0.017 g, 0.0086 mmol), N_3TEG[3a] (0.019 g, 0.086 mmol) and sodium ascorbate (0.015 g, 0.077 mmol) were dissolved in THF (1 mL) in a 10 mL Schlenk flask under Ar atmosphere. $CuSO_4$ (0.001 g, 0.0039 mmol) was added and the mixture was stirred vigorously for 2 days at 40°C. The solvent was removed *in vacuo*, and the product was extracted into 5 mL of DCM and stirred with EDTA (40 mg) for 2 hours. This process was repeated twice, and the solution mixture was dried over Na_2SO_4 and filtered. The solution was concentrated to 1mL *in vacuo*, and Et_2O was added dropwise to precipitate the oily product. The orange oil was dissolved in DCM (1 mL) and the precipitation was repeated another 2 times. The remaining DCM was removed *in vacuo* to yield a yellow oily film (0.034g, 61%). ^{1}H NMR (300MHz, $CDCl_3$): δ 3.58 (s, broad, 186H), 4.48 (s, broad, 8H), 4.58 (s, broad, 12H), 5.28 (s, broad, 24H), 7.48 (s, broad, 8H), 8.08 (s, broad, 12H) ppm. Expected mass: 3948.18 g·mol^{-1}, MALDI m/z = 3955.47 g·mol^{-1}.

2.2.9 G1-3-Cy5.5$_A$ (9): G1-3-TEGOH (**6**, 0.0946 g, 0.0804 mmol) and Cy5.5$_A$ analogue[1d] (0.170 g, 0.246 mmol) were dissolved in dry DCM (8 mL) in a 50 mL Schlenk flask under Ar in the dark. DMAP (0.0442 g, 0.362 mmol) was added and the mixture was stirred for 5 minutes. EDC (0.0412 g, 0.265 mmol) was added and the mixture was stirred for 2 days. The crude product was extracted in DCM (30 mL) and washed with water (1 x 10 mL) and brine (1 x 10 mL) and dried over $NaSO_4$. The solvent was removed *in vacuo*. The crude product was purified using neutral alumina for liquid chromatography with

DCM/MeOH (99:1) to remove the first band and DCM/MeOH (90:10) to obtain the product. The mixture was concentrated *in vacuo* to give blue-green powder (0.255g, 99%). ^{1}H NMR (300MHz, $CDCl_3$): δ 1.19-1.22 (m, 20H), 1.49 (s, 9H), 1.68-1.74 (m, 12H), 1.83 (s, 22H), 1.95 (s, 3H), 2.04 (s, 16H), 2.20 (s, 12H), 2.28-2.37 (m, 18H), 3.11 (s, 6H), 3.20-3.26 (m, 8H), 3.55-3.67 (m, 42H), 3.81-3.87 (d, 9H), 4.02-4.16 (d, 6H), 4.41-4.54 (t, 9H), 4.63 (s, 5H), 5.18 (s, 6H), 5.27 (s, 2H), 6.06 (d, 5H), 6.47 (s, 25H), 7.18 (t, 2H), 7.26-7.30 (m, 6H), 7.42 (s, 11H), 7.55 (s, 6H), 7.71 (d, 2H), 7.88 (s, 13H), 8.02 (t, 8H), 8.16 (s, 20H) ppm. ^{13}C NMR (300MHz, CDCl3): δ 23.66, 24.42, 26.28, 27.27-27.57, 29.63, 33.68, 43.98, 45.45, 49.96, 51.14, 63.45, 69.29, 70.39, 102.39, 109.34, 110.24-110.64, 122.04, 124.94, 126.27, 127.63, 128.17, 129.88, 130.69, 131.76, 139.25, 139.88, 143.07, 149.30, 152.01, 154.11, 173.20. Expected mass: 3194.92 g·mol^{-1}, ESI m/z = 3195.81 g·mol^{-1}.

2.3 Conjugation of ligands to gold nanoshells:
The thiol entity in the desired ligand was deprotected using the general procedure[3a] outlined here for G1-3TEGOH: the thioacetated ligand (0.118 g, 0.1 mmol) was dissolved in dry MeOH (2 mL) and sodium thiomethoxide (0.007 g, 0.1 mmol, 1M solution in MeOH) was added. The reaction was stirred for 3 hours. $HCl_{(aq)}$ (2 mL, 0.1 M) was added to the mixture. The product was extracted in DCM and washed with H_2O and brine, dried over $MgSO_4$ and concentrated *in vacuo* to yield the free thiol terminated ligand (0.072g, 63%). The deprotected ligand was reacted *in situ* for conjugating to the HAuNSh as follows. A freshly sonicated and Ar-purged concentrated solution of HAuNSh (3 mL) was mixed with the thioacetate-deprotected ligand under Ar atmosphere. MeOH (1 mL) was added to increase the solubility of the ligand. The mixture was stirred overnight in the dark. The solution of conjugated HAuNSh was diluted with a solution of trisodium citrate (1.7 mM) and then concentrated by centrifugation at 4600 rpm at 4°C for 3 hours before removing the supernatants and recombining the separate pellets. The conjugated HAuNSh were diluted once again with the trisodium citrate solution, and the process was repeated twice. In the case of highly colored ligands, the supernatant became progressively clearer with each wash and was completely colourless after the third and final wash, indicating that all unbound ligand had been removed. The concentrated conjugated AuNSh solution (approx. 3 mL) was stored in the dark at 4°C.

2.4. Photoacoustic Tomography
Solutions of HAuNSh and their functionalized analogues were filled in a polyethylene tube (0.4 X 0.2 X 0.1 mm; O.D X I.D X W.T) which was sealed on both ends and immersed in water at a depth of ~3 mm. Ultrasound (US) and photoacoustic (PA) imaging of the nanoparticle samples were performed using Vevo L AZR Photoacoustic Imaging System (Visual Sonics, ON, Canada) with LZ250 imaging probe (16MHz central frequency). US and PA images were acquired using a 680 nm laser and analyzed using Vevo workstation software.

2.5. Cellular imaging
2.5.1 Cell culture
J774 Mouse monocyte/macrophages and brain endothelial cells (bEnd.3) were cultured (at a density of $3x10^4$ cells/cm^2) in DMEM medium supplemented with 10% fetal bovine serum and incubated at 37°C, 5% CO_2 in a humidified atmosphere. After overnight incubation the cells were treated for 4h with G1-3-Cy5.5$_A$, G1-3-Cy5.5$_A$-HAuNSh or HAuNSh. At the end of the incubation time, the plates were thoroughly washed thrice with PBS (pH-7.4) to remove any unbound HAuNSh samples and fixed with 2% paraformaldehyde (in PBS pH 7.4) for 30 min at room temperature. The cells were again washed three times with PBS and mounted using 0.2% DABCO/glycerol (Sigma Aldrich, D2522, R6513).

2.5.2 Confocal microscopy
Cellular imaging was carried out using the LSM 710 AxioObserver confocal microscope (Carl Zeiss, Oberkochen, Germany) in the visible excitation wavelengths (excitation wavelengths = 633 nm). The fluorescence emissions were collected using a 697 nm long pass filter, to transmit only Cy5.5 emission. The images were acquired using Plan Apochromatic 40 × 1.3 oil immersion objectives.

2.6 Cellular uptake quantification
The cellular uptake was quantified using inductively coupled plasma – optical emission spectroscopy (ICP-OES). After 4 h treatment with HAuNSh and their conjugates, the cell plates were thoroughly washed 3 times with PBS to remove unbound nanoparticles, trypsinized and pelleted. The cell pellets were digested using concentrated HNO_3 and diluted with NanoQ water to make a final 5% HNO_3 concentration and then filtered through 0.22μm filter. ICP-OES was performed using an Agilent Technology 5100 ICP-OES spectrometer (Agilent Technology Inc, CA, USA). The cellular internalized [Au] was measured using a standard curved plotted by taking various concentration of Au standard (# 13881, Alfa Aesar) using λmax = 242.795 nm.

3. Results and Discussion
3.1 Ligand Synthesis
Design of the branched architectures employed in this study is based on our continued efforts to develop nanocarriers which impart aqueous solubility, biocompatibility, as well as enhanced efficiency in introducing multiple functional groups into a single platform.[3a,11] We have now developed a methodology to synthesize dendrons with a thiol entity at the core and variable TEG groups at the periphery. One of the hydroxyl groups of TEG was first selectively converted to a thioacetate. To achieve this, it was tosylated by reacting *p*-toluenesulphonyl chloride with a large excess of TEG under high dilution and at low temperature. The resulting monotosylated TEG (TEG-Ts, (**1**)) is activated towards nucleophilic substitution, and was replaced with thioacetate using the one-step procedure reported by Sato et al.[10] TEG-Ts (**1**) was reacted with commercially available potassium

thioacetate in dry DMF at room temperature for 12h under Ar. Although the original procedure states that no purification is needed besides a short work up, column chromatography was necessary to purify TEG-SAc (**2**). The thioacetate was found to degrade if left for long periods of time on a column, most probably due to the acidic nature of silica. Therefore, it was important that the purification of all subsequent compounds containing a thioacetate group is carried out relatively quickly, with column chromatography not lasting more than 3h. TEG-SAc was isolated as light brown-red oil and either used immediately or stored for a short period of time under inert atmosphere at 4°C.

Scheme 1 shows the synthetic procedure adopted for the construction of desired branched ligands containing thiol terminal entities. The core molecule (**4**) containing a carboxylic group and three acetylenes was prepared using a methodology reported earlier.[12] TEG-SAc (**2**) was coupled to **4** using Steglich esterification to yield the desired thiol group at the focal point (**5**). The resulting compound was subsequently reacted with three equivalents of TEG-Azide using copper catalyzed alkyne azide click (CuAAC) reaction in THF. The reaction was left to stir for 2 days, after which the product was extracted into DCM and stirred with EDTA to remove copper.[13] The product, G1-3-TEGOH (**6**), was purified by precipitation by adding Et_2O dropwise to a solution of the crude product dissolved in a minimal amount of DCM. The excess N_3-TEG gets into the Et_2O phase, and the product precipitates out. In our opinion, this method of purification is a much better alternative to column chromatography.

The synthetic procedure was further elaborated to the next generation of the dendron by reacting compound **4** in slight excess with **6** using an esterification reaction. G1-3-TEGOH (**6**), **4** and DMAP were dissolved in dry DCM and stirred for 5 minutes (Scheme 2). EDC was then added and the mixture was stirred for 2 days under an Argon atmosphere. The crude product was purified by column chromatography using DCM/MeOH mixture. The product was then reacted with nine equivalents of TEG-azide using CuAAC conditions. The mixture was stirred in THF for 2 days and then extracted in DCM. It was then washed twice with EDTA to remove any residual copper. The product was further purified by precipitation as described earlier for G1-3-TEGOH to give G2-9-TEGOH (**8**) in 61% yield.

One of the advantages these branched ligands offer is to incorporate different functionalities onto the surface of HAuNSh. The terminal hydroxyl groups in these dendrons can be used to covalently link any small molecule terminated with a carboxylic acid using esterification reaction.

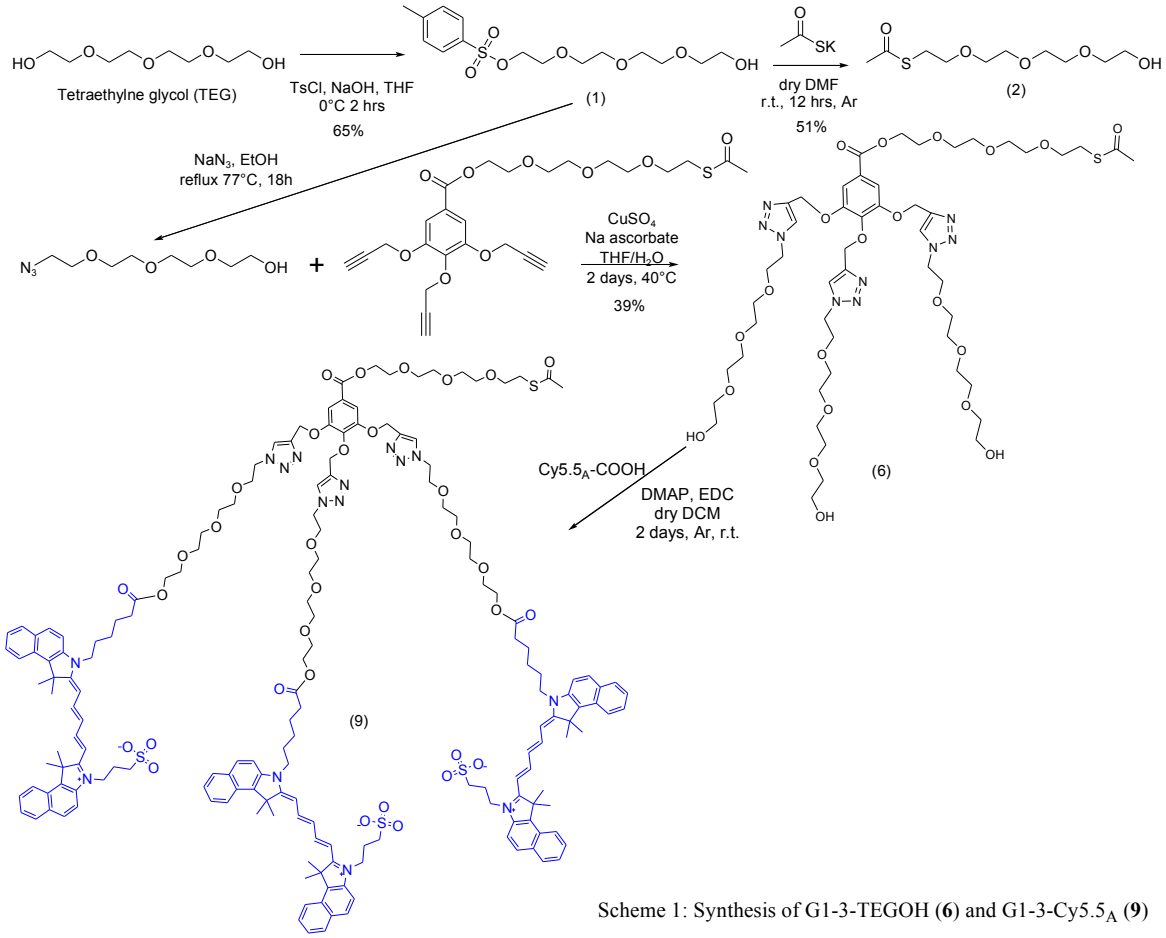

Scheme 1: Synthesis of G1-3-TEGOH (**6**) and G1-3-Cy5.5$_A$ (**9**)

We demonstrated the versatility of this methodology by functionalizing G1-3-TEGOH with a fluorescent dye ($Cy5.5_A$). G1-3-TEGOH, $Cy5.5_A$ and DMAP were dissolved in dry DCM and stirred for 5 minutes (Scheme 2).Then, EDC was added and the mixture was stirred for 2 days under Argon. The crude product was extracted into DCM and washed with water and brine, and then with $NaSO_4$. Column chromatography was used to purify the crude product. It was necessary to use alumina to pack the column since silica was found to degrade $Cy5.5_A$. It was interesting to note that the product was not an oil as in the case of G1-3-TEGOH, but a brittle blue-green powder. Although the yield was quite high (99%), the mass spectrum showed evidence of some mono- and di-functionalized compounds as well. The product was thus reacted further with the dye in an effort to complete the reaction. The mass spectrum showed an increase in the product; however, the other two compounds were still noted in minute amounts in the MS. The presence of the very small amount of this impurity was found to be useful, since it helped enhance the aqueous solubility of the dual imaging gold nanoshells based probe.

3.2 Ligand conjugation to gold nanoshells

The deprotection of the thioacetate group to yield the ligands which could be covalently linked to gold, was accomplished by adapting a procedure reported previously by Wallace and Springer.[14] This is a relatively mild method and tolerant of a number of functional groups including ester bonds and charged dye molecules such as $Cy5.5_A$. In a typical procedure, the protected compound was dissolved in dry methanol, cooled to 0°C, and one molar solution of sodium thiomethoxide in dry methanol was added. The reaction mixture was left to stir for 3-4 hours depending on the ligand. The monodentate ligand G0-TEGOH required 3 hours, while the G1-3-TEGOH (**6**), G2-9-TEGOH (**8**) and the G1-3- $Cy5.5_A$ (**9**) ligands required 4 hours for complete deprotection. Subsequently, a solution of 0.1 molar $HCl_{(aq)}$ was added to quench the reaction. The crude product was then extracted into DCM and washed with H_2O and brine. No further purification was performed since longer the deprotected compound was exposed to air, the stronger was the likelihood of forming disulfide bridges.[15] The reaction was monitored by ^1H NMR noted by the disappearance of the acetate group (typically found at 2.31 ppm). It should be noted that the G1-3-TEGOH ligand is difficult to solubilize after prolonged storage at 4°C under inert atmosphere since it yields a gel-like consistency. For compound **9**, ^1H NMR and UV-Vis confirmed that the $Cy5.5_A$ dye did not degrade under the deprotection conditions. The resulting deprotected compounds were immediately reacted *in situ* with a solution of HAuNSh, due to sensitivity of the thiol group to dimerization on exposure to air.

Gold nanoshells utilized in this study were prepared using the procedure reported earlier,[3a,4a] and it involved cobalt as a sacrificial template. In brief, cobalt(II) chloride hexahydrate was reduced with sodium borohydride ($NaBH_4$) in the presence of trisodium citrate. Gold (aurochloric acid) was then reduced onto this cobalt template. As the gold forms a shell structure around the nanoparticle, the cobalt is oxidized and diffuses through the pores into the aqueous solution, and yields the desired hollow gold nanoshell structure.

The deprotected mono or multidentate ligands were mixed with the gold nanoshell solution in a round-bottom flask under an inert atmosphere. Since prolonged storage increases the

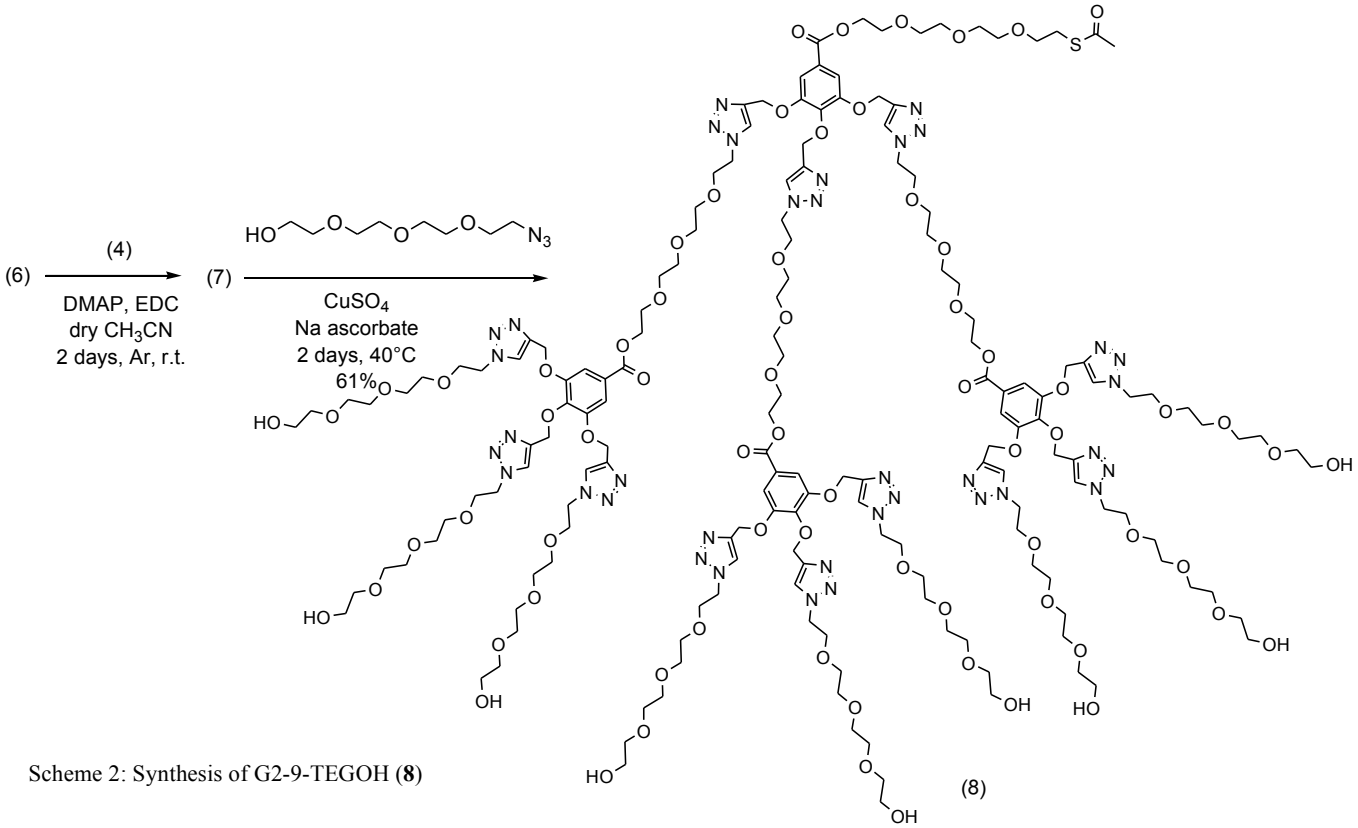

Scheme 2: Synthesis of G2-9-TEGOH (**8**)

likelihood of settling and aggregation of HAuNSh,[3a] the solution was sonicated prior to conjugation to ensure complete dispersion. In addition, argon was bubbled through the solution to remove oxygen, which would promote the formation of disulfide bonds. To ensure complete solubilisation of the ligand and a better coverage of the nanoshells, the ligands were first dissolved in 1-2 mL of dry MeOH and stirred for one minute before the addition of gold nanoshell solution. The formation of the Au-S bond is quite rapid; however the reaction was left to stir overnight to ensure complete conjugation.[16]

Following the overnight conjugation reaction, the functionalized HAuNSh were subjected to 3 centrifugation cycles at 4600 rpm at 4°C for 3h.[3a] Several precautions were taken to reduce the loss of conjugated nanoshells due to adherence to the centrifugation tube walls. First, a citrate buffer solution (using the same concentration of citrate as during the synthesis of the gold nanoshell themselves) was used to wash the conjugated HAuNSh as opposed to MilliQ water. This was found to reduce the adherence of nanoshells onto the surface of the plastic tubes.[3a] Second, the nanoshell pellets were transferred to new tubes after each centrifugation cycle. The combination of these precautionary measures resulted in almost no loss due to adherence or aggregation onto the plastic walls of the centrifugation tubes. After the centrifugation cycles, the conjugated gold nanoshell solutions were stored in MilliQ water at 4°C in the dark. The behaviour of these solutions in storage varied depending on the ligand. The more hydrophilic ligands (G1-3-OH, TEGOH) resulted in complete suspension of the nanoshells for several weeks. On the other hand, HAuNSh conjugated to hydrophobic ligands (G1-3-Cy5.5$_A$) gradually (but never completely) separated from the aqueous supernatant over the course of a few days. However, gentle shaking resulted in immediate resuspension of conjugated HAuNSh regardless of the identity of the ligand. For each conjugation reaction, the supernatant was collected for further analysis. The solvent was evaporated using a stream of air, and the solid residue was dissolved in a minimal amount of water and stored at 4°C.

3.2.1 G1-3-TEGOH (6) conjugation to gold nanoshells

Gold nanoshells were characterized using a combination of techniques including UV-Vis spectroscopy, transmission electron microscopy (TEM) and TGA. Upon conjugation with the G1-3-TEGOH ligand, the absorption maxima of the gold nanoshell solution blue shifted (from 742 to 714 nm) with a broadening of the peak (Figure 1). The latter was observed upon conjugation of all ligands to HAuNSh in this study, and may be attributed to the polydispersity in the binding of the ligands, i.e., not all of the nanoshells will have the same amount of ligands bound to their surface. This would result in a population that is not uniform.

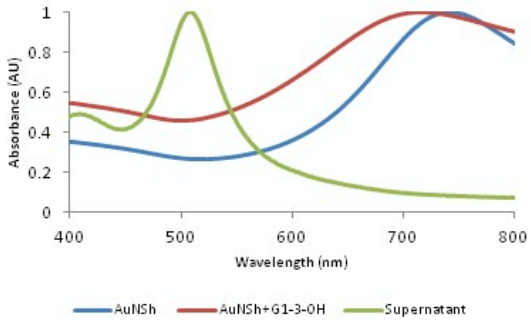

Figure 1: UV-Vis absorbance spectra of HAuNSh, conjugated with G1-3-TEGOH, and the supernatant solution.

Another explanation for the broadness is an increased amount of aggregation of the conjugated nanoshells which is occasionally visible by TEM (Figure 2). Before conjugation, the nanoshells were found to be 52±7 nm in diameter on average with a shell thickness of 6±2 nm, and after conjugation, 50±6 nm in diameter with a shell thickness of 6±2 nm. A thin film was observed around conjugated HAuNSh, and it was particularly visible when several nanoshells were in contact with each other. Another feature which was noted post-conjugation was the greater prevalence of nanoshells with defects such as what appeared to be holes (Figure 2c).

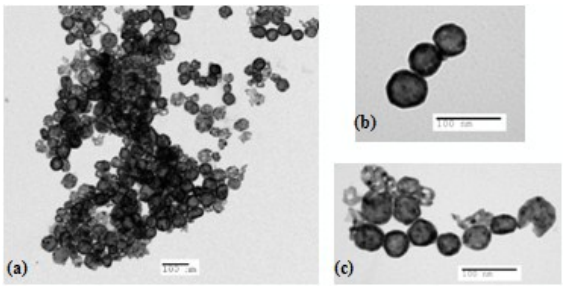

Figure 2. TEM images of HAuNSh conjugated with G1-3-TEGOH.

TGA analysis of the gold nanoshells depicted a weight loss onset at 150°C, and 51% of the mass loss was attributed to the organic ligand. It corresponds to ~226,387 ligands per nanoshell with a packing density of 27 ligands·nm^{-2}.[3a] Contrary to bare nanoshells which precipitate out of solution in just a short time, nanoshells conjugated with G1-3-TEGOH stayed in solution for an extended amount of time (one week), and were readily dispersed again after gentle shaking. This is attributed to the presence of three TEG groups on the ligand which increase aqueous solubility of the conjugated nanoshells.

During conjugation of ligands, major attention is generally paid to HAuNSh collected upon centrifugation, and the supernatant solution is often discarded. We were intrigued to examine and carry out an analysis of what remained in solution upon conjugation, and from the washings of the conjugated nanoshells. The supernatant was collected and evaporated under a steady stream of air. The resulting dark green residue was dissolved in a minimal amount of water. We were surprised to note that the supernatant residue dissolved so easily in water,

since our previous attempts to redissolve bare nanoshells in water once taken out of solution (through lyophilisation) had proved unsuccessful. The supernatant residue solution was characterized using the same techniques as the conjugated HAuNSh. Intriguingly, the UV-Vis spectrum was characteristic with absorbance peaks (~409, 509 nm) corresponding to particles that were smaller than those found in HAuNSh with both pre- and post-conjugation. The TEM analysis of this supernatant residue showed it was mainly comprised of a collection of small non-hollow nanoparticles of 5 ± 1 nm in diameter (Figure 3). However, there were also what appeared to be nanoshells in the process of rupturing into smaller nanoparticles (Figure 3b, c). The sizes of these nanoshells were roughly similar to those found in the centrifuged HAuNSh, *i.e.* 47±11 nm in diameter and 6±9 nm in shell thickness. The population present in the supernatant was estimated to be ~10-20% of the total amount of nanoshells used for conjugation. These features and structures found in the supernatant were not present in the TEM images of centrifuged conjugated nanoshells.

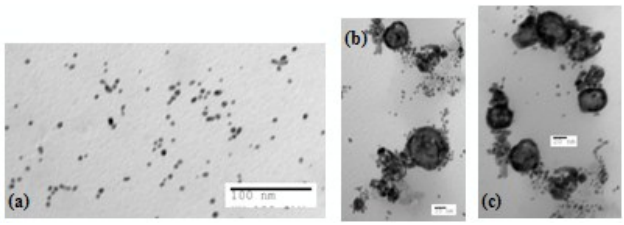

Figure 3. TEM images of the supernatant residue upon conjugation of G1-3-TEGOH to the HAuNSh.

Several hypotheses were considered to explain the observed changes in size and the breaking phenomenon of the HAuNSh leading to smaller gold nanoparticles seen in the TEM images of the supernatant. It should be noted that the damaged nanoshells were more prevalent in the supernatant of the conjugated nanoshell solution, and were not found in the bare nanoshell solution before carrying out the ligand displacement reaction on the surface of HAuNSh. One possibility could be that the centrifugation process – which is used to wash and remove unbound ligand post-conjugation – might have played a role in the breaking of the nanoshells. Perhaps the large ligand encountered resistance as the conjugated nanoshells were being driven to the bottom of the centrifuge tube. As a result of fluid dynamics, the ligand would then detach a small subset of the nanoshell which could explain the small particles visible in the TEM images of the supernatant. If this were the case, the breaking would be dependent on the speed of centrifugation. To test this hypothesis, gold nanoshells were conjugated with G1-3-OH, and split into 3 smaller batches. The latter were then subjected to different centrifuge speeds: 4600 rpm (the regular speed), 3600 rpm, and 2600 rpm. After completing these three centrifugation cycles for all three subsets, the solutions (and their supernatants) were characterized using UV-Vis and TEM. No significant morphological changes were observed in the TEM images; no speed favoured the prevalence of broken or porous HAuNSh. The UV-Vis spectra were similar in shape and absorbance maxima, with only a slight blue shift noticed between the highest and the lowest centrifugation speeds (Figure S1, Table ST1). These results suggest that the centrifugation force does not play a role in the breaking of conjugated HAuNSh.

It is possible that the large size of G1-3-TEGOH does not compensate for the displaced capping citrate agent on the bare nanoshells.[17] Citrate is known to be an excellent capping agent and provides structure and stability through a unique 3-dimensional assembly through ionic bonds.[18] G1-3-TEGOH is significantly larger than citrate, and perhaps displaces more than one citrate molecule, causing a void where the stability and integrity of the nanoshell is now impaired. This is perhaps the cause for the collapsing and rupturing of HAuNSh that are observed in the TEM images of the supernatant, as well as the higher prevalence of nanoshells with defects post-conjugation.

3.2.2 G0-TEGOH conjugation to gold nanoshells

We were intrigued by the results obtained upon functionalization of the gold nanoshells with the branched G1-3-TEGOH ligand, and decided to investigate the conjugation of its monofunctional linear analogue, G0-TEGOH. Upon binding HO-TEG-SH, the absorbance maximum of the HAuNSh blue shifted slightly from 604 to 601 nm (Figure S2), and there was broadening of the absorbance peak after conjugation. The absorption shift (Δ = 3 nm) was less pronounced than the one observed upon binding G1-3-TEGOH. TEM analysis showed that the monofunctional ligand conjugated HAuNSh were close in proximity to one another without aggregating into amorphous shapes (Figure S3). No significant changes in HAuNSh diameter and thickness were noted upon conjugation. Nanoshells conjugated with G0-TEGOH did not show any defects, unlike those conjugated with G1-3-TEGOH. As in the case of HAuNSh functionalized with G1-3-TEGOH, G0-TEGOH conjugated gold nanoshells were also easily dispersed in water and stayed in solution for extended periods of time (one week) with only gentle shaking necessary to redisperse them.

Upon TGA analysis, 37% of the mass loss was attributed to the organic ligand (with an onset temperature of 200°C). This corresponded to 147,415 ligands per nanoshell with a packing density of 63 ligands·nm^{-2}. This may suggest that G1-3-TEGOH ligand provides more coverage than the smaller TEGOH, and could be explained by considering that G1-3-TEGOH has three TEG units per sulphur binding site. The weight loss onset temperature was higher for G0-TEGOH functionalized gold nanoshells, and is perhaps due to the network structure observed in the TEM images.

The supernatant solution of the G0-TEGOH conjugation reaction was collected and evaporated to dryness. The residue thus collected was found to easily dissolve in water. Upon analyzing this supernatant residue solution, the results were found to be markedly different. The supernatant was populated by a collection of nanoshells, the sizes of which were roughly the same as those collected by centrifugation (Figure 4). High resolution-TEM (HR-TEM) showed that these nanoshells are

complete with shell thickness of 5±2 nm and a diameter of ~40 nm. They have crystal lattice structure of (111) for *fcc*-Au with a lattice plane of ~0.23 nm. The presence of Au was confirmed by an EDS analysis (Figure 4).

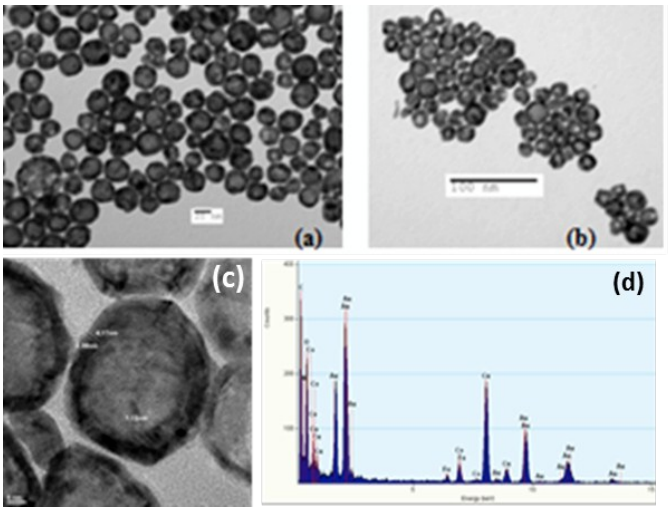

Figure 4. TEM image of the HAuNSh conjugated wih G0-TEGOH (a), the supernatant residue (b), high resolution-TEM image (C) with shell thickness and ligand coating. (D) Energy dispersive x-ray spectroscopy (EDS) analysis of the HAuNSh-G0-TEGOH.

There were virtually no non-hollow nanoparticles as observed in the supernatant of conjugated G1-3TEGOH gold nanoshells. The fact that we observed no breaking of nanoshells post-conjugation both in the supernatant and the conjugated nanoshell solution, it suggests that the size of the ligand plays an important role in disturbing the stability and integrity of HAuNSh. G0-TEGOH is significantly smaller than G1-3-TEGOH, and more comparable to citrate in size. It is quite possible that one TEGOH molecule is able to replace one citrate entity upon conjugation, and thus keeps the integrity of the nanoshell intact.

3.2.3 G2-9-TEGOH conjugation to gold nanoshells

G2-9-TEGOH was conjugated to HAuNSh following the same procedure as described above for G0-TEGOH and G1-3-TEGOH ligands. UV-Vis analysis of the conjugated gold nanoshells exhibited extensive broadness and plateau of the absorbance peak (Figure S4), and their TEM images were similar to those of nanoshells conjugated with G1-3-TEGOH. The nanoshells were present in small groups and a significant number of them presented defects (Figure S5). The nanoshell dimensions did not change much upon conjugation (before conjugation 40±4 nm in diameter with a shell thickness of 5±2 nm; and after conjugation, 41±5 nm in diameter with a shell thickness of 5 ± 2 nm). TGA analysis showed that 35% of the mass loss was due to the organics which corresponds to 34,433 ligands per nanoshell with a packing density of 7 ligands·nm^{-2}. The low packing density is attributed to the size of the ligand. Although the presence of 9 TEG units should significantly increase coverage, but we reach a limit in terms of how many of these large ligands can occupy the surface of a single gold nanoshell. HAuNSh conjugated with G2-9-TEGOH had a higher onset temperature (230°C) than either G0-TEGOH (200°C) or G1-3-TEGOH (150°C). This implies that G2-9-TEGOH was more difficult to remove from the surface of nanoshells than the other two ligands.

TEM analysis of the supernatant from the conjugation of G2-9-TEGOH to HAuNSh revealed nanoshells similar to those in the supernatant of the nanoshells conjugated with G1-3-TEGOH. They had a large number of defects, and several appeared to be in the process of rupturing or collapsing (Figure 5). The sizes of these nanoshells were roughly the same as those removed upon centrifugation. There was also a very small amount of non-hollow nanoparticles of 4±1 nm. The population of gold nanoshells present in the supernatant was similar to the ones noted for G1-3-TEGOH (10-20% of the amount of the total amount of conjugated nanoshells).

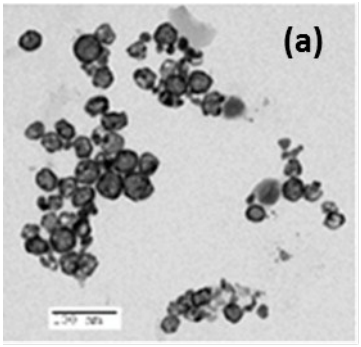

Figure 5. TEM image of the supernatant residue upon conjugation of G2-9-TEGOH to the HAuNSh.

3.2.4 Dual imaging probe: G1-3Cy5.5$_A$ conjugation to gold nanoshells:

Upon conjugating G1-3-Cy5.5$_A$ to HAuNSh, the absorbance maximum blue shifted from 816 to 644 nm (Δ = 107 nm), and a broadening of the peak was observed (Figure S6). A post-conjugation shift and broadening of this magnitude were not observed when conjugating any of the other ligands which do not have a dye attached to them. This is thought to be a consequence of the proximity of the dye Cy5.5$_A$ to the HAuNSh.[19] TEM images revealed small groups or single nanoshells, several of which presented defects (Figure 6).

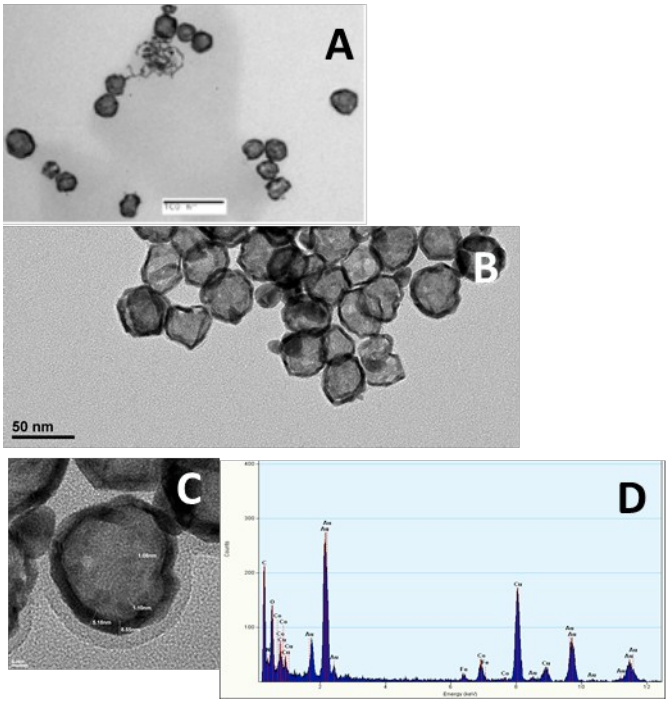

Figure 6: TEM image of HAuNSh conjugated with G1-3-Cy5.5$_A$ at low (A, B) and high resolution-TEM (C) with shell thickness and ligand coating; (D) Energy dispersive x-ray spectroscopy (EDS) analysis of the HAuNSh-G1-3-Cy5.5$_A$.

Before conjugation, the nanoshells were 43±6 nm in diameter with a shell thickness of 5±2 nm, and after conjugation 39±5 nm in diameter with a shell thickness of 5±2 nm (Figure 6A,B). After conjugation, the shell thickness and the shape of nanoshells remained almost the same with an additional 3.4 nm of the G1-3-Cy5.5$_A$ coating over the shell (Figure 6C). Grafting G1-3-Cy5.5$_A$ ligand on to the nanoshells retained the polycrystalline structure with different oriented well defined lattice fringes (~0.23 nm) corresponding to (111) lattice crystal plane for *fcc*-Au as observed previously.[3] EDS analysis further confirmed the presence of gold characteristic peaks (Mα and Lα at 2.12 and 9.17 keV) (Figure 6D). HAuNSh conjugated with G1-3-Cy5.5$_A$ were found to be soluble in water, and this is notable since Cy5.5$_A$ does not dissolve in water. This could be explained by considering that the mass spectrum of G1-3-Cy5.5$_A$ had indicated the presence of a minute amount of the mono- (G1-Cy5.5$_A$-2-TEGOH) and di-functionalized (G1-2-Cy5.5$_A$-TEGOH) ligands. The presence of TEG increases aqueous solubility of these conjugated nanoshells. An analysis of the supernatant showed that it contained mostly the unbound ligand, deformed nanoshells and small non-hollow nanoparticles. These observations are similar to the conjugation of branched G1-3-TEGOH and G2-9-TEGOH ligands to HAuNSh.

The fluorescence spectrum of nanoshells conjugated with G1-3-Cy5.5$_A$ was acquired and compared with that of the unbound ligand (Figure 7). To ensure that both spectra were comparable, solutions of the conjugated nanoshells and the free ligand were optimized to have the same absorbance (A=0.094). As absorbance scales linearly in the low concentration regime, both of these solutions would have approximately the same concentration of the ligand. As seen in Figure 6, upon conjugating, the proximity of the ligand to the gold nanoshell suppressed the fluorescence of the Cy5.5$_A$ dye.

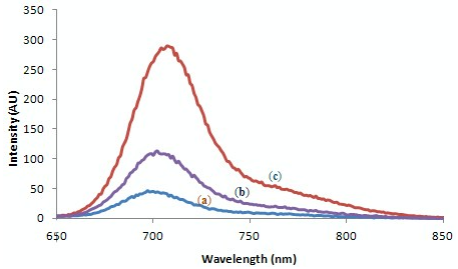

Figure 7. Flourescene spectra of HAuNSh conjugated with G1-3-Cy5.5$_A$ (a); G1-3-Cy5.5$_A$-HAuNSh upon treatment with DTT for 24h (b); and G1-3-Cy5.5$_A$ (c).

In order to release the ligand from the surface of the nanoshells and restore fluorescence, a 0.8M solution of dithiothreitol (DTT) in MilliQ H_2O was prepared and gradually added to the solution containing the conjugated nanoshells, and allowed to react for 1h. Intriguingly, the fluorescence of Cy5.5$_A$ was not restored, suggesting that it was still bound to the HAuNSh. We hypothesized that it may simply be a kinetic issue, and DTT did not have sufficient time to fully displace the Cy5.5$_A$ ligands and restore fluorescence. Considering that G1-3-Cy5.5$_A$ ligand is quite bulky, it is conceivable that DTT would require more than a few minutes (the normal time in such displacement reactions), for it to reach the surface of HAuNSh to undergo a displacement reaction, and covalently bind to the gold surface (releasing G1-3-Cy5.5$_A$ and restoring its fluorescence). Indeed, when a solution of HAuNSh conjugated with G1-3-Cy5.5$_A$ was allowed to react with DTT for 24 hours, the fluorescence was found to increase (Figure 7) indicating the release of the ligand.

4.1 Photoacoustic properties

In vitro tests using commercially available Vevo LAZR, Visualsonics instrument were performed to examine the photoacoustic imaging properties of functionalised HAuNSh (Figure 8). The left column shows the ultrasound images and the right column, photoacoustic images. The photoacoustic images were acquired at two different wavelengths 680 and 770 nm. The photoacoustic intensity of HAuNSh (lane 2), HAuNSh-G0-TEGOH (lane 3), HAuNSh-G1-3-TEGOH (lane 4), G1-3-Cy5.5A-HAuNSh (lane 5) were compared with water at both the wavelengths. All the four samples (lanes 2-5) showed good photoacoustic signal intensity at 680 nm (Figure 8C). However, the signal intensity decreased for the sample G1-3-Cy5.5A-HAuNSh (lane 5) at 770 nm (Figure 8C,D). This is in accordance with the UV-VIS spectra as observed in Figure 1, indicating that ligand conjugation changed the plasmon resonance properties and absorption was blue shifted. This

indicates that the nanoshells upon ligand functionalisation changes the PA signals, and can be employed as a platform feasible for the photoacoustic imaging using plasmonic gold nanoshells.

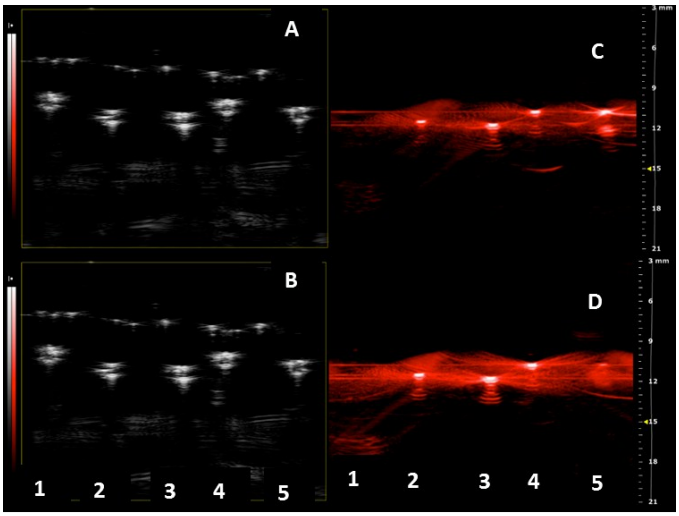

Figure 8. In vitro phantom containing HAuNSh and functionalized HAuNSh samples: Left: Ultrasound images (A,B); Right: Photoacoustic images (C,D) at 680 nm (upper panel) and 770 nm (lower panel). Phantoms: 1 – water, 2 – HAuNSh, 3 – HAuNSh-G0-TEGOH, 4 - HAuNSh-G1-3-TEGOH, 5 - G1-3-Cy5.5A-HAuNSh.

4.2 Cellular uptake and imaging studies

The cellular uptake of the HAuNSh and G1-3-Cy5.5$_A$-HAuNSh was examined using bright field microscopy (Figure 9). Both bEnd.3 and J774 cells showed no morphological changes after treatment with ~6μg/ml of HAuNSh and G1-3-Cy5.5$_A$-HAuNSh for 4 h. Both the cell types showed uptake of the HAuNSh as indicated by red arrows (Figure 9). As seen in column II, both the macrophages and endothelial cells uptake HAuNSh (red arrows). Similar observations were made after treatment with G1-3-Cy5.5$_A$-HAuNSh (column III). To clearly understand the extent of ligand functionalized and unfunctionalized HAuNSh uptake in the bEnd.3 and J774 after 4h treatment, ICP-OES analysis was performed.

As shown in Table 1, 60% of the treated HAuNSh are uptaken by J774 cells after 4 h. On the other hand, J774 cells had uptaken 67% of the G1-3-Cy5.5$_A$-HAuNSh. This suggests that the functionalized nanoshells are uptaken to a slightly greater extent than the unfunctionalized nanoshells. Endothelial cells had uptaken only 23% of the HAuNSh as compared to the ligand functionalized HAuNSh (63%). Table 1 clearly shows that J774 uptake both unfunctionalized and functionalized gold nanoshells to a greater extent than the endothelial cells. This explains the phagocytic behavior of the macrophages as compared to other cell types. Gold nanoparticles functionalized with different ligands have also been shown to display similar trends of cellular uptake by different macrophage cells.[20]

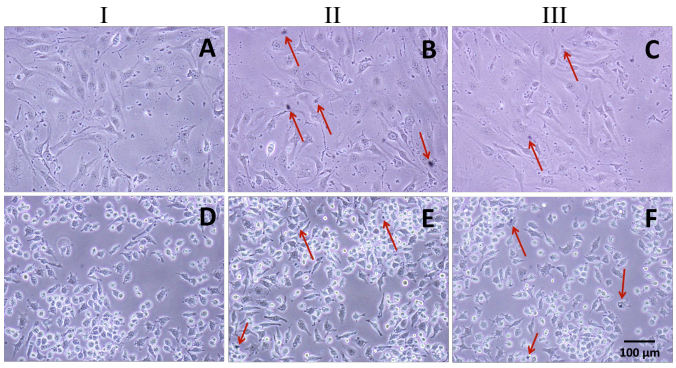

Figure 9: Optical images of bEnd.3 (A-C) and J774 cells (D-F). Column I: untreated cells, column II: treatment with HAuNSh, and column III: G1-3-Cy5.5$_A$-HAuNSh treatment. The red arrows indicate the presence of HAuNSh (B-E) and G1-3-Cy5.5$_A$-HAuNSh (C-F).

Table 1: Uptake of HAuNSh in J774 and bEND.s cells

	Treated concentration (μg/10^6 cells)	Uptaken concentration (pg)/cell	
		J774	bEnd.3
HAuNSh	6.5	3.9 (60%)	1.5 (23%)
G1-3-Cy5.5$_A$-HAuNSh	6.5	4.4 (67%)	4.1 (63%)

To investigate the intracellular localization of Cy5.5$_A$ based ligand (G1-3-Cy5.5$_A$) and its corresponding functionalized gold nanoshells (G1-3-Cy5.5$_A$-HAuNSh), fluorescence imaging experiments were performed using J774 and bEnd.3 cells following a 4h treatment. Unlabeled cells depicted normal morphology without any fluorescence (Figure 10A-C), and upon treatment with G1-3-Cy5.5$_A$ ligand, an intense fluorescence signal was observed. G1-3-Cy5.5$_A$ showed an even distribution in the cytoplasm without any labelling in the nucleus (Figure 10D-F). It indicates that the dye accumulates intracellularly without altering cell morphology. The bEnd.3 cells exposed to functionalized gold nanoshells (G1-3-Cy5.5$_A$-HAuNSh) showed no intracellular fluorescence (Figure 10 G-I). This is in agreement with the earlier observation that the fluorescence of G1-3-Cy5.5$_A$ is quenched upon conjugation to gold nanoshells. Similar fluorescence quenching of G1-3-Cy5.5$_A$ upon covalent linking to HAuNSh was observed in J774 macrophages (Figure S7). It has been reported that the quenching occurs when the fluorophore is confined within ~5nm distance from the nanoparticle surface,[21] and it relates mainly to the reduction in the radiative rate rather than energy transfer.[22] This phenomenon has also been observed in other studies at the biomolecular and cellular levels.[23] Our results demonstrate that with a ligand packing density of ~5-7

ligands/nm^2 on a 40 nm HAuNSh, the fluorescence signal of the linked Cy5.5$_A$ dye molecules is suppressed. Such multifunctional nanoprobes offer immense potential as ON-OFF sensors both at the molecular and cellular level.

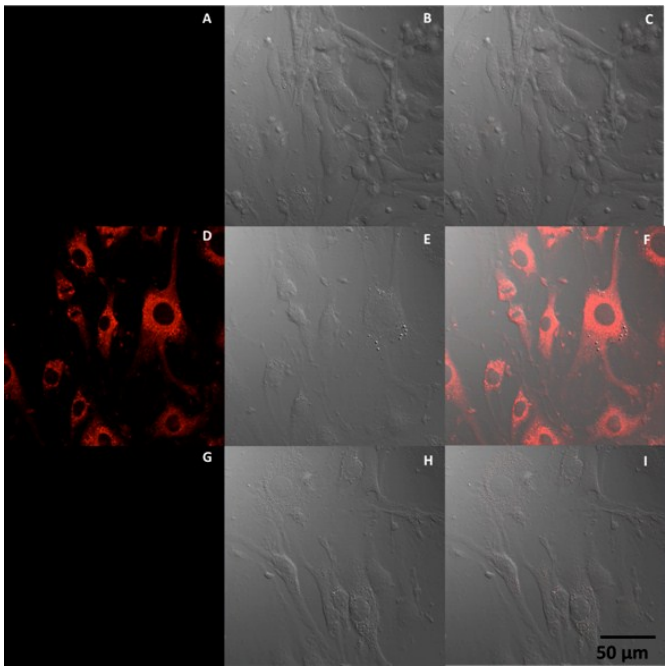

Figure 10: Confocal images of unlabeled brain endothelial cells (A–C), labeled with G1-3-Cy5.5$_A$ ligand (D–F) and G1-3-Cy5.5$_A$-HAuNSh (G–I) for 4h. The 3 column panels show the fluorescence (A,D,G), optical (B,E,H), and overlay of fluorescence and optical (C,F,I) images.

Conclusions

Functionalization of gold nanoshells with appropriate ligands for applications in a variety of areas including biology, theranostics etc., constitutes a topical area of research. Branched multivalent ligands provide a platform to enhance the efficacy of surface coverage by introducing multiple units in one step. We have examined the conjugation of TEG based linear and dendron ligands to HAuNSh through their terminal thiol moiety. Introduction of TEG on the surface of gold nanoshells enhances their aqueous solubility. In the events leading up to the functionalization of the gold nanoshells with branched dendron ligands and in contrast to the linear analog, we were intrigued to find ruptured HAuNSh as well as small non-hollow gold nanoparticles in the supernatant. The examination of the often discarded supernatant suggests that the size plays a very important role in this routinely used substitution reaction. The displacement of small citrate molecules is not compensated by the addition of one large dendritic ligand, generating a void and compromised shell integrity. Our results also suggest that the branched architecture offers more coverage, and enhances aqueous solubility of the HAuNSh. Using the methodology outlined here, we constructed gold nanoshells which offer dual imaging modality. The covalent linking of the Cy5.5$_A$ dye to gold nanoshells quenches its fluorescence. The release of the dye with the often used DTT ligand required longer time probably due to the steric protection offered by dendron based ligands. Our study provides a simple and versatile platform to design a variety of multi-tasking nanoprobes including the dual imaging modality demonstrated here.

Acknowledgements

We would like to thank Natural Sciences and Engineering Research Council (Canada), Fonds de Recherche du Québec - Nature et technologies (FRQNT, Quebec, Canada), and Center for Self-assembled Chemical Structures (FQRNT, Quebec, Canada) for financial support.

Notes and references

[a]*Department of Chemistry, McGill University, 801 Sherbrooke St. West, Montreal, Quebec H3A 0B8 Canada. Fax: +514-398-3797; Tel: +514-398-6912; E-mail: ashok.kakkar@mcgill.ca.*
[b]*Institute of Biomedical Engineering, École Polytechnique de Montréal, 2900, boul Édouard-Montpetit, Montreal, H3C 3A7, Canada Fax: 514-340-4611; Tel: +514-340-4711; E-mail: frederic.lesage@polymtl.ca.*
[c]*Montreal Heart Institute, Research Center, 5000 Bélanger Est, Montréal, Quebec H1T 1C8, Canada Tel:+514-376-3330, ex. 3091. E-mail: Eric.Rheaume@icm-mhi.org.*
[d]*Université de Montréal, Institute of Biomedical Engineering, Department of Physiology, P.O. Box 6128, Station Centre-Ville, Montreal, Quebec, H3C 3J7 Canada.*
[e]*Département de génie chimique et de génie biotechnologique, 2500, Boulevard Université, Université de Sherbrooke, Sherbrooke, Québec, J1K 2R1, Canada. Tel : +1-514-821-8000 ext . 62758. E-mail : Leonie.Rouleau@USherbrooke.Ca*
[f]*Département of Medicine, Université de Montréal, Montreal, Quebec, Canada*
[§]These two authors contributed equally.
†Footnotes should appear here. These might include comments relevant to but not central to the matter under discussion, limited experimental and spectral data, and crystallographic data.
Electronic Supplementary Information (ESI) available: Additional UV-Vis spectral, TEM and centrifugation speed data, and confocal images. See DOI: 10.1039/b000000x/

1 (a) Z. Laing, X. Li, Y. Xie, S. Liu, *Biomed. Mater.* 2014, **9**, 025012; (b) A. J. Coughlin, J. S. Ananta, N. Deng, I. V. Larina, P. Decuzzi, J. L. West, *Small*, 2014, **10**, 556-565; (c) D. Sikdar, I. D. Rukhlenko, W. Cheng, M. Premaratne, *Nanoscale Res Lett.* 2013, **8**, 142-148; (d) L. Rouleau, R. Berti, V. W. Ng, C. Matteau-Pelletier, T. Lam, P. Saboural, A. K. Kakkar, F. Lesage, E. Rheaume, J. C. Tardif, *Contrast Media Mol Imaging*, 2013, **8**(1), 27-39; (e) C. Bao, N. Beziere, P. del Pinto, B. Pelaz, G. Estrada, F. Tian, V. Ntziachristos, J.M. de la Fuente, D. Cui, *Small*, 2013, **9**(1), 68-74; (f) C. Zhang, Z. Zhou, Q. Qian, G. Gao, C. Li, L. Feng, Q. Wang, D. Cui, *J. Mater. Chem. B*, 2013, **1**, 5045-5053; (g) D. A. Giljohann, D. S. Seferos, W. L. Daniel, M. D. Massich, P. C. Patel, C. A. Mirkin, *Angew Chem Int Ed Engl* 2010, **49** (19), 3280-3294; (h) T. A. Erickson, J. W. Tunnell, *Nanomaterials for the Life Sciences Vol 3: Mixed Metal Nanomaterials*, C. S. S. R. Kumar, Ed., 2009, Wiley-VCH, Verlag GmbH & Co., Weinheim; (i) M. Hu, J. Chen, Z-Y. Li, L. Au, G. V. Hartland, X. Li, M. Marquez, Y. Xia, *Chem Soc Rev* 2006, **35** (11), 1084-1094; (j) M. L. Brongersma, *Nature Materials*, 2003, **2**, 296-297; (k) E. Prodan, P. Nordlander, N. J. Halas, *Nano Lett* 2003, **3**, 1411.

2 (a) C. Sauerbeck, M. Haderlein, B. Schurer, B. Braunschweig, W. Peukert, R.N. Klupp Taylor, *ACS Nano*, 2014, **8**(3), 3088-3096; (b) J.C.Y. Kah, N. Phonthammachai, R.C.Y. Wan; J. Song; T. White; S. Mhaisalkar, I. Ahmad, C. Sheppard, M. Olivo, *Gold Bulletin*, 2008, **41**, 23-36; (c) H.-P. Liang, L.-J. Wan, C. L. Bai, L. Jiang, *J. Phys Chem B* 2005, 109, 7795; (d) H.-P. Liang, L.-J. Wan, C. L. Bai, L. Jiang, *J. Phys Chem B* 2005, **109**, 7795; (e) S. L. Westcott, S. J. Oldenburg, T. R. Lee, N. J. Halas, *Cheml Phys Lett* 1999, **300**, 651-655.

3 a) V.W.K. Ng, P.K. Avti, M. Bedard, T. Lam, L. Rouleau, J-C Tardif, E. Rheaume, F. Lesage, A. Kakkar, *J. Mater. Chem. B.* 2014, **2**, 6334-6344; (b) M. P. Melancon, W. Lu, Z. Yang, R. Zhang, Z. Cheng, A. M. Elliot, J. Stafford, T. Olson, J. Z. Zhang, C. Li, *Mol. Cancer Ther.* 2008, **7**(6), 1730-1739; (c) B.G. Prevo, S.A. Esakoff, A Mikhailovsky, J.A. Zasadzinski, *Small*, 2008, **4**, 1183-1195.

4 (a) A. M. Schwartzberg, T. Y. Olson, C. E. Talley, J. Z. Zhang, *J. Phys Chem B* 2006, **110**, 19935; (b) J. Turkevich, P. C. Stevenson, J. Hillier, *Discuss Faraday Soc.* 1951, **11**, 55.

5 (a) R. Raghavendra, K. Arunachalam, S.K. Annamalai, A.M. Arunachalam, *Int. J. Pharm. Sci.* 2014, **6**, 74-87; (b) R. Bardhan, S. Lal, A. Joshi, N. J. Halas,. *Acc Chem Res* 2011, **44**, 936; (c) Z. Li, P. Huang, X. Zhang, J. Lin, S. Yang, B. Liu, F. Gao, P. Xi, Q. Ren, D. Cui, D. *Mol Phar* 2010, **7**, 94; (d) G. B. Braun, A. Pallaoro, G. Wu, D. Missirlis, J. A. Zasadzinski, M. Tirrell, N. O. Reich, *ACS Nano* 2009, 3, 2007. (e) G. Wu, A. Milkhailovsky, H. A. Khant, C. Fu, W. Chiu, J. A. Zasadzinski, *J. Am. Chem. Soc.* 2008, **130**, 8175; (f) W. Cai, T. Gao, H. Hong, J. Sun, *Nanotechnol. Sci. Appl.* 2008, **1**, 10.2147/NSA.S3788, 1-25; (g) P. K. Avti, D. Maysinger, A. Kakkar, *Molecules* 2013, **18**, 9531.

6 (a) B. Moses, Y. You, *Med. Chem.* 2013, **3**, 192-198; (b) Z. J. Deng, M. Liang, I. Toth, M. J. Monteiro, R. F. Minchin, *ACS Nano* 2012, **6**, 8962; (c) C. Freese, M. I. Gibson, H. A. Klok, R. E. Unger, C. J. Kirkpatrick, *Biomacromolecules* 2012, **13**, 1533; (d) E.C. Dreaden, M.A. Mackey, X. Huang, B. Kang, M.A. El-Sayed, *Chem. Soc. Rev.* 2011, **40**, 3391-3404; (e) Z. Liang, Y. Liu, X. Li, Q. Wu, J. Yu, S. Luo, L. Lai, S. Liu, *J Biomed Mater Res A* 2011, **98**, 479.

7 (a) J.P. Hermes, F. Sander, U. Fluch, T. Peterle, D. Thompson, R. Urbani, T. Pfohl, M. Mayor, *J. Am. Chem. Soc.* 2012, **134**, 14674-14677; (b) C. Peng, K. Li, X. Cao, T. Xiao, W. Hou, L. Zheng, R. Guo, M. Shen, G. Zhang, X. Shi, *Nanoscale*, 2012, **4**, 6768-6778; (c) J. R. Baker Jr., *Hematology*, 2009, **1**, 708-719.

8 (a) H. Chen, M. Zhang, H. Yang, W. Xu, Y. Ma, Y. Gu, *RSC Adv.* 2014, DOI : 10.1039/C3RA47453D; (b) M. Kacenka, O. Kaman, J. Kotek, L. Falteisek, J. Cerny, D. Jirak, V. Herynek, K. Zacharovova, Z. Berkova, P. Jendelova, J. Kupcik, E. Pollert, P. Veverka, I. Lukes, *J. Mater. Chem.* 2011, **21**, 157-164; (c) Z. Wang S. Zong, J. Yang, J. Li, Y. Cui, *Biosens. Bioelectron*. 2011, **26**, 2883-2889. (d) W. Chen, R. Bardhan, M. Bartels, C. Perez-Torres, R. G. Pautler, N.J. Halas, A. Joshi, *Mol. Cancer Ther.* 2010, **9**, 1028; (e) S. Lee, X. Chen, *Molecular Imaging*, 2009, **8**, 1536-0121.

9 (a) M.-C. Daniel, M. E. Grow, H. Pan, M. Bednarek, W. E. Ghann, K. Zabetakis, J. Cornish, *New J Chem* 2011, **35**, 2366; (b) H. Gao, K. Matyjaszewski, K. *J. Am. Chem. Soc.* 2007, **129**, 6633; (c) A. Sharma, G. M. Soliman, N. Al-Hajaj, R. Sharma, D. Maysinger, A. Kakkar, *Biomacromolecules* 2011, 13, 239; (d) P.R. Ashton, J. Huff, S. Menzer, I.W. Parsons, J.A. Preece, J.F. Stoddart, M.S. Tolley, A.J.P. White, D.J. Williams, *Chemistry - A European Journal* 1996, **2**, 31.

10 Y. Sato, K. Yoshioka, M. Tanaka, T. Murakami, M. N. Ishida, O. Niwa, *Chem. Comm.* 2008, **40**, 4909.

11 (a) L. Albertazzi, F.M. Mickler, G.M. Pavan, F. Salomone, G. Bardi, M. Panniello, E. Amir, T. Kang, K.L. Killops, C. Brauchle, R. Amir, C.J. Hawker, *Biomacromolecules* 2012, **13**, 4089; (b) Y. Umeda, C. Kojima, A. Harada, H. Horinaka, K. Kono, *Bioconjugate Chemistry* 2010, **21**, 1559. (c) X. Huan, D. Wang, R. Dong, C. Tu, B. Zhu, D. Yan, X. Zhu, *Macromolecules* 2012, **45**, 5941.

12 J. Camponovo, J. Ruiz, E. Cloutet, D. Astruc, *Chemistry - A European Journal*, 2009, **15**, 2990.

13 L. Wang, D.J. Kiemle, C.J. Boyle, E.L. Connors, I. Gitsov, *Macromolecules* 2014, **47**, 2199.

14 O.B. Wallace, D.M. Springer, *Tetrahedron Letters* 1998, **39**, 2693.

15 X.-B. Li, Z.-J. Li, Y.-J. Gao, Q.-Y. Meng, S. Yu, R.G. Weiss, C.-H. Tung, L.-Z. Wu, *Angew. Chem. Int. Ed.* 2014, **53**, 2085.

16 R.L. Whetten, R.C. Price, *Science* 2007, **318**, 407.

17 (a) D.-H. Tsai, M.P. Shelton, F.W. DelRio, S. Elzey, S. Guha, M.R. Zachariah, V.A. Hackley, V. A. *Analytical and Bioanalytical Chemistry* 2012, **404**, 3015; (b) S.V. Kumar, S. Ganesan, *International Journal of Green Nanotechnology* 2011, **3**, 47.

18 J.-W. Park, J.S. Shumaker-Parry, *J. Am. Chem. Soc.* 2014, **136**, 1907.

19 (a) F. Zhang, J. Zhu, J.-J. Li, J.-W Zhao, *Applied Physics Letters* 2013, **103**, 193703/1; (b) A.-M. Gabudean, F. Lerouge, T. Gallavardin, M. Iosin, S. Zaiba, O. Maury, P.L. Baldeck, C. Andraud, S. Parola, *Optical Materials*, 2011, **33**, 1377.

20 (a) R. Shukla, V. Bansal, M. Chaudhary, A. Basu, R.R. Bhonde, M. Sastry. *Langmuir* 2005, **21**, 10644-10654; (b) K. Ye, J. Qin, Z. Peng, X. Yang, L. Huang, F. Yuan, C. Peng, M. Jiang, X. Lu. *Nanoscale Res Lett* 2014, **9**, 529; (c) T.A. Larson, P. P. Joshi, K. Sokolov. *ACS Nano* 2012, **6(10)**, 9182.

21 (a) E. Dulkeith, A. C. Morteani, T. Niedereichholz, T.A. Klar, J. Feldmann, S. A. Levi, F. C. J. M. van Veggel, D. N. Reinhoudt, M. Moller, D. I. Gittins. *Phys. Rev. Lett* 2002, **89**, 203002-1-4; (b) K. Aslan, V. H. Perez-Luna. *J. Fluoresc* 2004, **14**, 401–405.

22 E. Dulkeith, M. Ringler, T.A. Klar, J. Feldmann, A. M. Javier, W. J. Parak. *Nano Lett* 2005, **5,** 585–589.

23 (a) A. E. Prigodich, D. S. Seferos, M. D. Massich, D. A. Giljohann, B. C. Lane, C. A. Mirkin. *ACS Nano* 2009, **3**, 2147–2152; (b) C. C. You, O. R. Miranda, B. Gider, P. S. Ghosh, I. B. Kim, B. Erdogan, S. A. Krovi, U. H. F. Bunz, V. M. Rotello. *Nat. Nanotechnol* 2007, **2**, 318–323; (c) A. Bajaj, O. R. Miranda, I. B. Kim, R. L. Phillips, D. J. Jerry, U. H. F. Bunz, V. M. Rotello. *P. Natl. Acad. Sci. USA* 2009, **106**, 10912–10916; (d) D. J. Maxwell, J. R. Taylor, S. M. Nie SM. *J. Am. Chem. Soc* 2002, **124**, 9606–9612.

Graphical Abstract:

Conjugation of multivalent ligands to gold nanoshells and designing a dual modality imaging probe

Mathieu Bedard, Pramod K. Avti, Tina Lam, Leonie Rouleau, Jean-Claude Tardif, Eric Rhéaume, Frederic Lesage and Ashok Kakkar

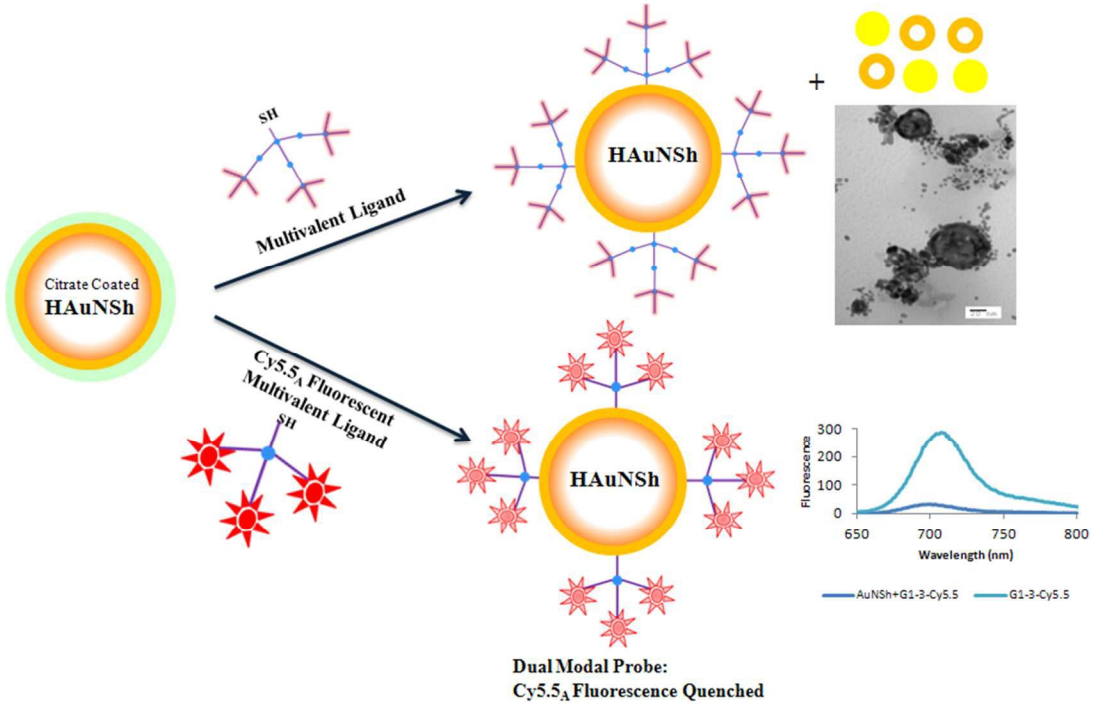

Hollow gold nanoshells functionalized with branched multivalent ligands provide an excellent platform to develop nanoprobes with dual imaging capabilities.